Comprehensive study of the surface peak in charge-integrated low-energy ion scattering spectra

M. Draxler,[1] R. Beikler,[2] E. Taglauer,[2] K. Schmid,[1,2] R. Gruber,[1] S. N. Ermolov,[1,3] and P. Bauer[1]
[1]*Johannes-Kepler Universität Linz, Institut für Experimentalphysik, A-4040 Linz, Austria*
[2]*Max-Planck-Institut fuer Plasmaphysik, EURATOM Association, D-85748 Garching bei Muenchen, Germany*
[3]*Institute of Solid State Physics, Russian Academy of Sciences, Chernogolovka, Moscow District 142432, Russia*
(Received 31 January 2003; published 20 August 2003)

Low-energy ion scattering is very surface sensitive if scattered ions are analyzed. By time-of-flight (TOF) techniques, the neutral and the charge-integrated spectra (ions plus neutrals) are obtained, which yield information about deeper layers. It is well known that charge integrated spectra may exhibit a surface peak which is more pronounced for heavier projectiles, e.g., Ne ions. Aiming at a more profound physical understanding of this surface peak, we performed TOF experiments and computer simulations for H, He, and Ne projectiles scattered from a polycrystalline copper target. Measurements were done in the range of 1–9 keV for a scattering angle of 129° under UHV conditions. The simulations were performed using the MARLOWE code for the given experimental parameters and a polycrystalline target. In the experiments, a pronounced surface peak was observed at low energies, which fades away at higher energies. This peak is quantitatively reproduced by the simulation. Several atomic layers may contribute to the surface peak, depending on the energy. Analyzing the contributions of the individual outermost atomic layers, one finds that the binary collisions of the projectiles with atoms in the first and the second layer yield a narrow energy distribution, while the contribution from the deeper layers is dominated by multiple scattering and therefore exhibits a very broad energy spectrum. It is shown that the appearance of a more or less pronounced surface peak is due to the relative contributions of single scattering and multiple scattering and thus depends on the projectile energy and mass.

DOI: 10.1103/PhysRevA.68.022901 PACS number(s): 79.20.Rf

I. INTRODUCTION

Ion scattering is a standard tool for quantitative surface and thin-film analysis and includes a large variety of experimental techniques such as Rutherford backscattering (RBS) [1,2], elastic recoil detection [3], and low-energy ion scattering (LEIS) [1,4]. These techniques make use of a wide energy range of the projectiles ($\sim$1 keV–100 MeV) and are all based on the same physical mechanism: ions are used as projectiles and the energy spectra of either the backscattered projectiles or the recoiling atoms are measured at a large scattering angle θ. Thus, detected particles have undergone a close encounter. Let us in the following concentrate on RBS and LEIS, where the energy spectra of scattered ions are measured. They contain two different types of information: the energy transfer from the projectile to the recoil atom in the close collision yields information on the mass of the scattering center, and the energy lost by the projectile along its path due to electronic interaction yields information on the depth in which the scattering took place [5].

The interpretation of the ion spectra along these lines is based on the single-scattering model, which assumes that the projectile path consists of two straight lines that represent the incoming and outgoing trajectories and intersect at the position where the scattering takes place. Within this model, the width of the energy spectrum of the scattered projectiles is well defined; there is a well-defined highest energy, i.e., kE_0, where k is the kinematic factor that describes the energy lost in the binary collision and E_0 denotes the incident energy. In addition, the energy loss dE of the projectile per path length dx inside the target is described by the electronic stopping power $S=dE/dx$ [6]. Within the surface energy approximation [5], projectiles that impinge at an angle α with respect to the surface normal, that are backscattered at a depth Δx, and that leave the target under an angle β with respect to the surface normal are detected at an energy E_x, given by

$$E_x = k\left(E_0 - \frac{S(E_0)\Delta x}{\cos\alpha}\right) - \frac{S(kE_0)\Delta x}{\cos\beta}. \quad (1)$$

Thus, the spectrum width ΔE is proportional to the scattering depth and the stopping power factor $[S(\alpha,\beta,k,E_0)]$, defined by the following equation:

$$\Delta E = \left[\frac{kS(E_0)}{\cos\alpha} + \frac{S(kE_0)}{\cos\beta}\right]\Delta x \equiv [S(\alpha,\beta,k,E_0)]\Delta x. \quad (2)$$

The single-scattering (SS) model is valid as long as the probability for additional scattering of the projectile by a significant angle along its trajectory is negligible. Thus, the model is most appropriate in the regime of high energies and small depths; the lower the energy is, the more important are the plural scattering (PS) and the multiple scattering (MS). There is no strict way to differentiate between PS and MS. A qualitative way to visualize PS and MS is to think of MS when scattering occurs by angles smaller than the half-width angle of the MS distribution, $\alpha_{1/2}$ [7], and of PS when the scattering angles are larger than $\alpha_{1/2}$. A typical PS event involves scattering by roughly 90°, and at least one additional scattering such that the projectile finally reaches the detector, while as a consequence of MS, the mean path length is increased and the large-angle scattering event becomes less well defined [8]. A comprehensive treatment of the influence of MS and PS on the shape of an RBS spectrum was presented by Smit [9]. For the case of He ions and a Cu target, the increasing importance of PS and MS at low ener-

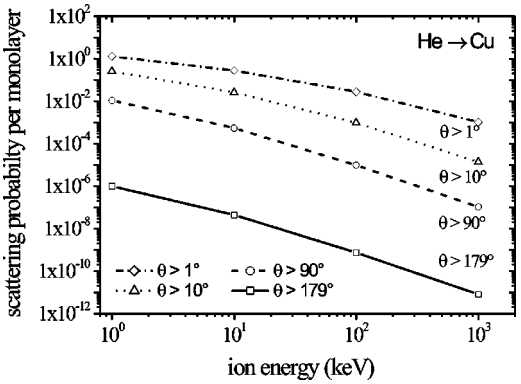

FIG. 1. Scattering probability per monolayer of He ions from copper atoms.

gies is visualized in Fig. 1, where the probability is shown for scattering in a monolayer by an angle larger than 1°,10°,90°, and 179°, respectively. From this figure, it becomes clear that in the RBS regime ($E_0 \approx 1$ MeV) the single-scattering model is quite appropriate, while in the LEIS regime ($E_0 \approx 1-10$ keV) PS and MS become important even for targets with a thickness of the order of 10 monolayers. As a consequence, in LEIS the relation between the final energy of the projectile and the depth is not as well defined as in the RBS regime. Only for the ions detected at kE_0, the single-scattering model is still valid, since only the projectiles that are scattered by the surface atoms can be detected as ions. Even if reionization contributes, this does not cause fundamental problems since reionized ions are detected at lower energies.

From what is said above, it is clear that it was quite a surprise for the scientific community that also in charge-integrated LEIS spectra, a more or less pronounced surface peak was observed, depending on the type of projectile (see, e.g., Ref. [10]). While for H ions hardly any surface peak is observed (see also Ref. [11]), for He ions a pronounced peak is observed at low energies, and for heavier ions such as Ne the surface peak may be a dominant feature of the total spectrum. There were speculative attempts to explain the origin of this surface peak in neutral (charge-integrated) LEIS spectra. However, so far it has not been really understood. In Ref. [10], an explanation in terms of channeling was suggested, but it was not discussed why protons would not show any channeling. It is interesting to think about the possible mechanisms to create such a surface peak in a backscattering spectrum. A surface peak appears, if (at least) one of the following conditions are met: (i) the number of visible atoms, N, is higher in the surface than in the deeper layers ($N_1 > N_{n>1}$); (ii) the stopping power is lower at the surface than in the deeper layers ($dE/dx|_1 < dE/dx|_{n>1}$); (iii) the stopping power is higher at the surface than in the deeper layers ($dE/dx|_1 > dE/dx|_{n>1}$); (iv) the energy-loss straggling Ω [12] is lower at the surface than in the deeper layers ($\Omega_1 < \Omega_{n>1}$). The prototypic example for condition (i) is channeling. The absence of MS and PS in the surface layer and their onset in the deeper layers (see below) are an example for condition (ii); also the Lewis effect in excitation curves near narrow nuclear resonances [13] is related to condition (ii). Condition (iii) is hardly met anywhere, but the monolayer resolution obtained in RBS is based on a large energy loss per monolayer under the grazing incidence conditions. The fact that in high-resolution RBS the surface peak is best resolved while severe damping is observed for the deeper layers, this is due to condition (iv). In Fig. 2, mechanisms (i) to (iv) are visualized for a hypothetical case, where the spectrum consists of a number of Gaussians, one Gaussian corresponding to one atomic layer.

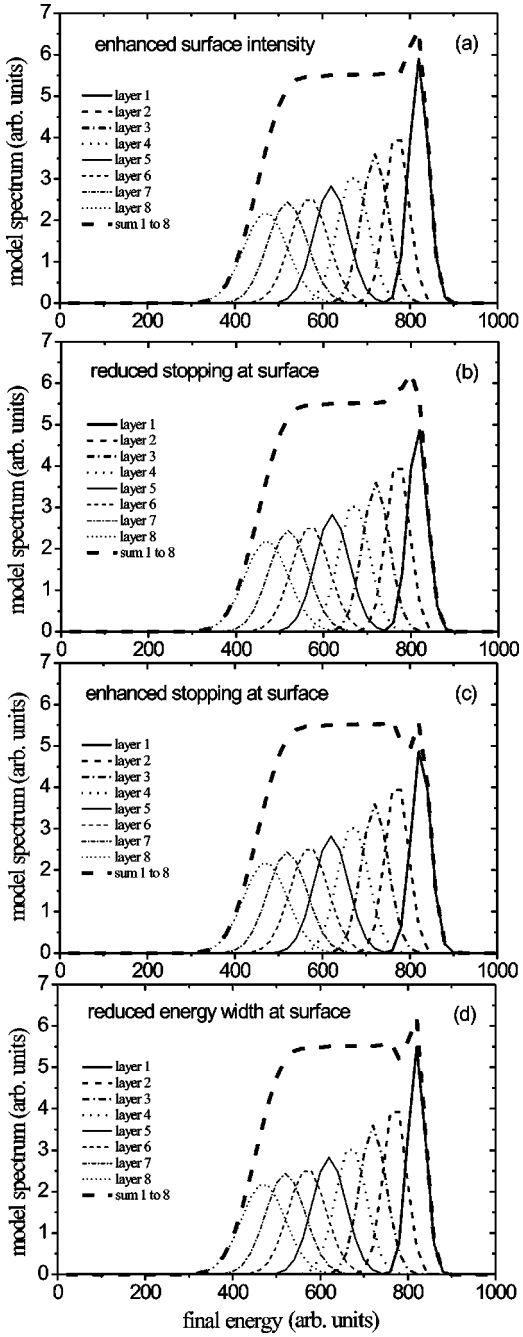

FIG. 2. Possible mechanisms creating surface peaks.

The aim of the present paper is to explain the physical origin of the observed surface peak. For this purpose, time-of-flight (TOF) experiments and computer simulations using the MARLOWE code were performed, as described below.

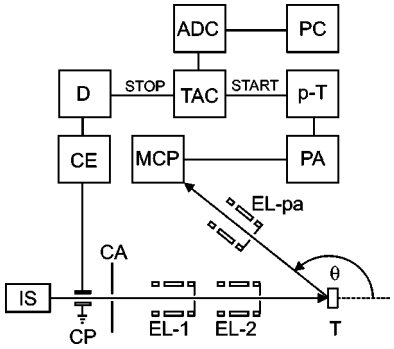

FIG. 3. Schematic view of our TOF-LEIS (see also text) is shown, and is explained in the following. ADC is the analog-to-digital converter, CA is the chopper aperture, CE is the chopper electronic, CP shows the chopper plates, D shows the delay, EL-1 and EL-2 are the electrostatic lenses, EL-pa is the electrostatic lens usable for postacceleration, IS is the ion source, MCP is the microchannel plate, PA is the preamplifier, PC is the personal computer, *p-T* is the picotiming discriminator, T is the target, TAC is the time-to-amplitude converter, and θ is the scattering angle.

II. EXPERIMENT AND SIMULATION

Figure 3 shows our TOF-LEIS setup, which has been described elsewhere [14] and thus will be just summarized here. A beam of monoatomic ions (e.g., H^+,He^+,Ne^+, . . .) is produced by an ion source in the energy range of 500 eV-10 keV with an energy uncertainty of $\approx 0.8\%$. The beam is mass analyzed by means of a velocity filter with a mass resolution $M/\Delta M \approx 400$. An electrostatic chopper is used to produce the required beam packets with a time width that can be varied in steps of 25 ns, the minimum packet length being ≈ 40 ns. Two Einzel lenses focus the beam onto the target [15,16], typical beam diameters at the target are 1 mm. Care was taken to ensure a beam diameter <2 mm, in order to guarantee a beam spot smaller than the pupil of the TOF analyzer. In the flight path between the target and the stop detector, positive ions can be postaccelerated by a negative potential applied to the drift tube, thereby permitting to separate the ions from the neutrals in the spectrum. Without postacceleration, charge-integrated spectra are recorded.

In order to minimize the flow of the gas from the ion source to the target chamber, several differential pumping stages are installed. The base pressure in the UHV target chamber is $\leqslant 2\times 10^{-10}$ mbars. In order to the prevent neutral projectiles to hit the target, a 3° kink is implemented in the beam line. Scattered projectiles are detected at an angle of 129° by means of a TOF-LEIS system, with a flight path of ≈ 1 m for the primary beam, and a flight path $L_f = 0.67$ m for the scattered particles. As stop detector, a stack of two microchannel plates was used, the entrance potential being -2400 V so that a detection efficiency for ions $>0.95\eta_0$ [17] is obtained, where η_0 denotes the probability to hit a sensitive part of the channel plate ($\eta_0 = 0.6$ in our case [18]). The detection electronics consists of standard components, i.e., a 1-GHz preamplifier (EG&G ORTEC 9306), a picotiming discriminator (EG&G ORTEC 9307), a time-to-amplitude converter/single-channel analyzer (EG&G ORTEC 567), and an analog-to-digital converter (CANBERRA 8713). The electronics is temperature stabilized to reduce thermal drifts as far as possible.

Two types of copper targets were used, a sheet of highly pure Cu and an evaporated Cu film; they were cleaned by sputter-annealing cycles. For sputtering, 1-keV argon ions were used, the annealing temperature was 650 K. Purity was checked by means of Auger-electron spectroscopy. After cleaning, no impurities were visible in the Auger spectrum. The target was mounted on a target manipulator that can hold two targets and permits three translations (x,y,z) and two rotations (polar angle and tilt). Thus, the angles of incidence and of exit can be varied in a wide range, which allow us to study the relative importance of the incoming and the outgoing trajectories on the scattered ion yield (see Ref. [19]). The target holder also allows us to measure the beam current in a Faraday cup and the total current (incoming beam and emitted electrons) at the target, and also holds a luminescent screen to check the size of the beam when changing the beam energy. The target is kept at ground potential in order to minimize distortion of the measured TOF spectra by electric fields.

The TOF spectra are converted to energy spectra following the standard procedure [20]. An ion of mass M_1 that leaves the target with an energy E_f (velocity v_f) needs a flight time T_f to pass the distance L_f to the detector. In the absence of any fields, the relation $E_f = (M_1/2)v_f^2 = (M_1/2)(L_f/T_f)^2$ holds, from which one obtains by particle conservation, $N(E_f)dE_f = N(T_f)dT_f$, the well-known relations for the energy spectrum $N(E_f)$ and for the energy resolution δE:

$$N(E_f) = N(T_f)dT_f/dE_f = N(T_f)\times 2E_f/T_f, \tag{3}$$

$$\delta E_f = 2\,\delta T E_f/T_f \propto \delta T E^{3/2}/M_1^{1/2}. \tag{4}$$

For example, for 2-keV He, $\delta T = 40$ ns correponds to $\delta E = 50$ eV and to a depth resolution $\delta x = \delta E/[S] = 10$ Å, using the (electronic) stopping power of Ref. [6].

With this setup, charge-integrated TOF-LEIS spectra were measured for our Cu targets and the following projectiles: He^+ at 1 keV, 3 keV, and 9 keV (see Fig. 4); and H^+ and Ne^+ at 3 keV (see Fig. 5). The spectra 3 keV were measured at perpendicular incidence, while the spectra at 1 and at 9 keV were obtained in different runs and at different geometries ($\alpha = 51°$ and 54° at 1 keV and 9 keV, respectively). In Figs. 4 and 5, also spectra are shown obtained from the experimental data by correction for the energy dependent detector efficiency [17], assuming identical efficiency for ions and neutrals [21]. In the following, we discuss efficiency corrected spectra only.

All He spectra and the H spectrum show a sharp onset at the binary collision energy kE_0, corresponding to backscattering from the surface. The shape at kE_0 is determined by the experimental resolution. The Ne spectrum extends to energies far above kE_0, due to PS (projectiles may reach the detector after having suffered several scattering events at angles $\ll\theta$). There is another indication that PS and MS are of less importance for H and He ions than for Ne ions: when the experimental spectra are compared to the single-

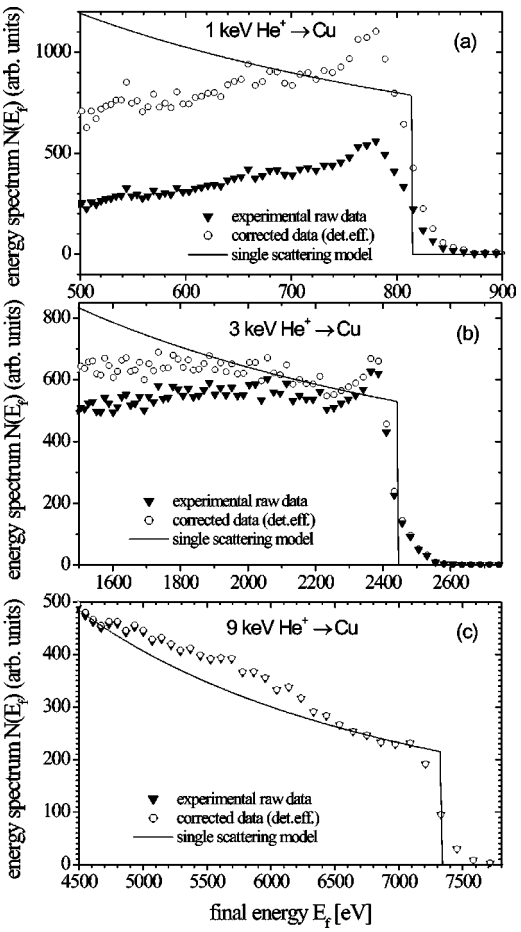

FIG. 4. Experimental spectra compared to the single-scattering spectra for 1-, 3-, and 9-keV He ions and Cu targets.

scattering spectra (obtained using Ziegler-Biersack-Littmark stopping [6] and a screened Coulomb potential [22]), as shown in Figs. 4 and 5, it is obvious that the only case where not even a qualitative agreement is obtained, is the case of Ne. This is related to the fact that for Ne ions the scattering potential is so strong that an impact parameter $b=a_0=0.529$ Å corresponds to a scattering angle $\theta=25°$, while it corresponds to $\theta=6°$ and $\theta=3°$ for He and H ions, respectively.

A prominent feature of the experimental spectra obtained for He and Ne ions is the existence of a more or less pronounced peak at kE_0, the so-called surface peak (see Figs. 4 and 5). For He, the relative height of the surface peak is largest at 1 keV, although it may be damped due to limited experimental resolution; it is weaker at 3 keV and not visible at 9 keV. For Ne ions, the surface peak is the dominant feature of the spectrum, while for H ions, it is not visible. The physical origin of this surface peak will be discussed in detail below.

Apart from this surface peak, the shape of the spectra for H and He ions is in accordance with the expectation; for H ions, the measured spectrum follows the single-scattering spectrum down to 1500 eV (see Fig. 4). For He ions, the agreement between the experiment and the single-scattering calculation depends on the primary energy; for $E_0=9$ keV,

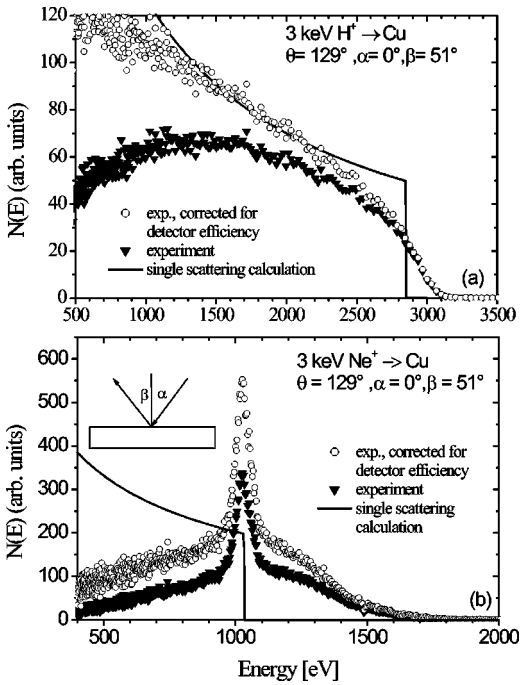

FIG. 5. Experimental spectra compared to the single-scattering spectra for 3-keV H and Ne ions backscattered from Cu targets.

the single-scattering spectrum fits the experimental spectrum fairly well down to $E_f \approx 4000$ eV [see Fig. 4(c)], the observed deviations being due to PS and MS. For $E_0=3$ keV, the range of final energies, where the measured spectrum is reproduced by the single-scattering calculation is smaller [down to $E_f \approx 1800$ eV, see Fig. 4(b)], reflecting a stronger influence of PS and MS. For the lowest primary energy $E_0=1$ keV, the single-scattering calculation seems to be appropriate in quite a narrow range of final energies only [down to $E_f \approx 680$ eV, see Fig. 4(a)]. This is in qualitative agreement with the expectation, since $\alpha_{1/2} \propto Z_1 Z_2 / E$, where Z_1 and Z_2 denote the atomic numbers of the projectile and the target, respectively [7].

The simulations were performed by using the computer code MARLOWE [23], which treats scattering as a series of binary collisions within classical mechanics. The polycrystalline target model was chosen, in which a single crystal is rotated after each collision by a random angle. As in the experiment, perpendicular incidence was chosen, and all the particles that were scattered into the interval $127.5° \leqslant \theta \leqslant 130.5°$ were registered. In order to obtain acceptable statistics, 2×10^6 trajectories were calculated for each spectrum.

III. RESULTS AND DISCUSSION

In Figs. 6(a)–6(c), our experimental results for 9-, 3-, and 1-keV He ions are compared to MARLOWE spectra, obtained as described above, for the identical scattering conditions as in the experiment. We discuss the general features of these spectra, and then deal in detail with the analysis of the surface peak.

For 9 keV, the experimental energy spectrum is very well reproduced by the MARLOWE spectrum in the whole simu-

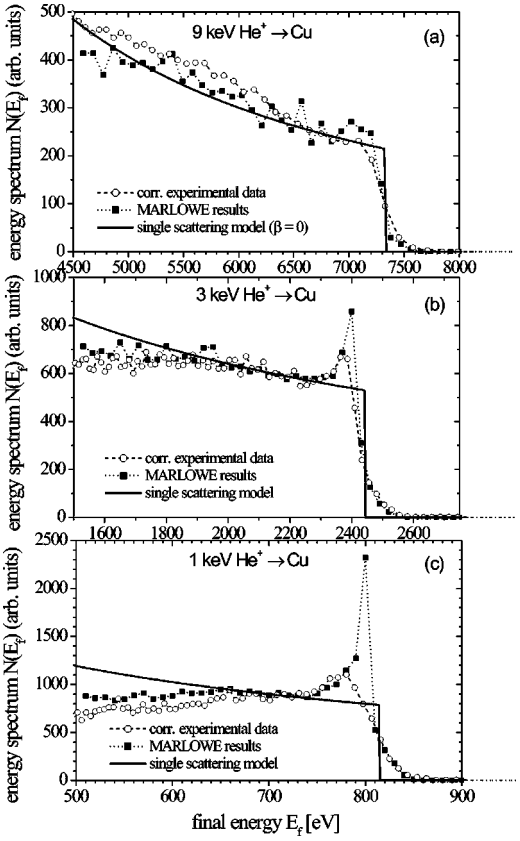

FIG. 6. Comparison of the experimental and the simulated spectra.

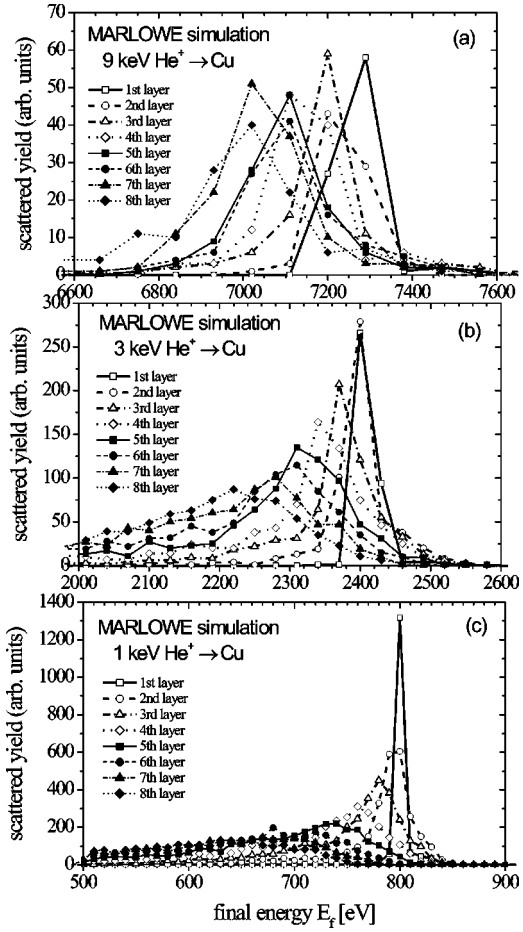

FIG. 7. Contributions of the eight outermost atomic layer to the simulated spectra.

lated energy range, i.e., from 4500 to 8000 eV [see Fig. 6(a)]. In the simulation, there is a small indication of a surface peak with a width of ≈ 350 eV, which is hardly visible since it exceeds the spectrum plateau by only three standard deviations. In the experimental spectrum, the energy resolution at the energy of ≈ 350 eV does not permit to resolve this peak.

In Fig. 6(b), for $E_0 = 3$ keV again a very good agreement is observed in the whole energy range for the MARLOWE simulation and the measured spectrum; both show a pronounced surface peak in a very narrow energy interval with a width of ≈ 70 eV around kE_0. In the experimental spectrum, the surface peak has a smaller height than in the simulated spectrum. This may be partly due to the inferior experimental resolution (≈ 70 eV) and partly due to the local electronic energy-loss model used in the simulation, which yields the same final energy for the projectiles after binary scattering from an atom in the surface layer and in the second layer, in contrast to what is expected from a nonlocal energy-loss model.

For 1-keV He, the agreement between the MARLOWE simulation and the measured data is again satisfactory in the whole simulated range of energies [see Fig. 6(c)]. At kE_0, the simulation exhibits a surface peak with a width of less than 10 eV, which exceeds the rest of the spectrum by a factor of 2 in height. The experimental surface peak is again less pronounced than the simulated one, as in Fig. 6(b). At energies below 650 eV, the simulated spectrum is higher than the experimental data by about 20%. This can be due to different reasons: in the simultation, either the scattering potential or the electronic energy loss are not sufficiently realistic, or the detection efficiency correction of the experimental data is inadequate at low energies.

In Fig. 6, the increasing importance of PS and MS with decreasing primary energy is visible in the experimental spectra as well as in the simulations at energies above kE_0; there is a tail due to PS at energies $E > kE_0$, and the relative intensity in the tail increases with respect to the spectrum height with decreasing energy.

Let us now discuss the surface peak. As stated before, the simulated surface peaks have an energy width of ≈ 350 eV, 70 eV, and 30 eV at $E_0 = 9$, 3, and 1 keV, respectively. These widths would correspond to a scattering depth of 12, 5.5, and 4 atomic layers, respectively, in the single-scattering approximation [22]. Since in the simulation kinematic broadening is considerable, these numbers represent a safe upper limit for the number of target layers contributing to this peak.

In order to look for the physical origin of this peak, we present in Figs. 7(a)–7(c) the energy distributions of the eight outermost atomic layers that build up the spectrum around kE_0, again for primary energies 9, 3, and 1 keV. What is common to all three plots is that the scattering by the surface layer always results in a very sharp binary collision peak, with an energy width that is limited just by the colli-

sional broadening due to the finite acceptance angle ($127.5° - 130.5°$). This is equivalent to the statement that PS and MS do not influence scattering from the surface layer. It is common to all the three plots that the deeper layers contribute peaks that are shifted to lower energies (due to electronic energy loss) and broadened. In the present regime, the broadening is mainly due to PS and MS. To a lesser extent also electronic straggling contributes to the broadening of the simulated spectra, but this broadening mechanism is not fully included in the calculation, as described above.

There are, however, qualitative differences visible in Figs. 7(a)–7(c); as expected, PS and MS become more important at lower energies, with half-width angles $\alpha_{1/2}$ of 4°, 12°, and 37° for 9, 3, and 1 keV, respectively. Accordingly, at 9 keV, the influence of PS and MS is very small so that all layers shown in Fig. 7(a) yield peaks that are well defined and separated from each other. Obviously, the width of the peak corresponding to the outermost surface layer is reduced with respect to the other layers ($\Omega_1 < \Omega_{n+1}$, see Introduction), and projectiles scattered by surface atoms may suffer a slightly reduced energy loss ($dE/dx|_1 < dE/dx|_{n>1}$). As a consequence, a small surface peak should be expected for 9-keV He. However, the depth resolution at 9 keV is rather bad (≈ 3 ML for the simulation and ≈ 12 ML for the experiment) so that the surface peak is hardly visible in the MARLOWE spectrum and invisible in the experiment.

At a primary energy of 3 keV, already for the second layer a tail due to PS is obtained at $E_f > kE_0$, and the subsurface contributions are much more broadened by PS and MS than for $E_0 = 9$ keV. In addition, the depth resolution at 3 keV is better than at 9 keV (≈ 5.5 ML for the simulation and ≈ 8 ML for the experiment). Both effects should result in the observation of a stronger surface peak, to which the first and the second layer contribute, in good agreement with the simulation and with experiment [see Fig. 7(b)].

Finally, at 1 keV the influence of PS and MS is so strong that even layers close to the surface yield a broad scattering spectrum with a width of hundreds of eV [see Fig. 7(c)]. With an energy resolution of ≈ 15 eV in the simulation and of ≈ 30 eV in the experiment, for 1-keV He, the depth resolution is good enough to resolve the spectrum shape in the surface peak region [see Fig. 6(c)], showing a large tail due to PS and an extremely sharp surface peak (with a width < 10 eV in the simulation) which is followed by a tail that merges the plateau of the spectrum. From Fig. 7(c), it becomes clear that the sharp peak is due to the surface layer contribution. The tail towards lower energies is due to the second and the third layer, while the deeper layers do not contribute to the surface peak.

Let us now discuss the measurements and simulations for protons and Ne ions at 3 keV. The resulting spectra are shown in Figs. 8(a) and 8(b). From Fig. 8(a), it is clear that for 3-keV protons the experiment is well described by the computer simulation (minor influence of MS and PS). It is also obvious that the experimental resolution is worse than in the case of 3 keV He^+ so that no surface peak is visible in the experiment, while a very narrow surface peak is obtained in the simulation. From Fig. 9(a), one easily can deduce that this peak is due to two reasons: (i) the peak which originates

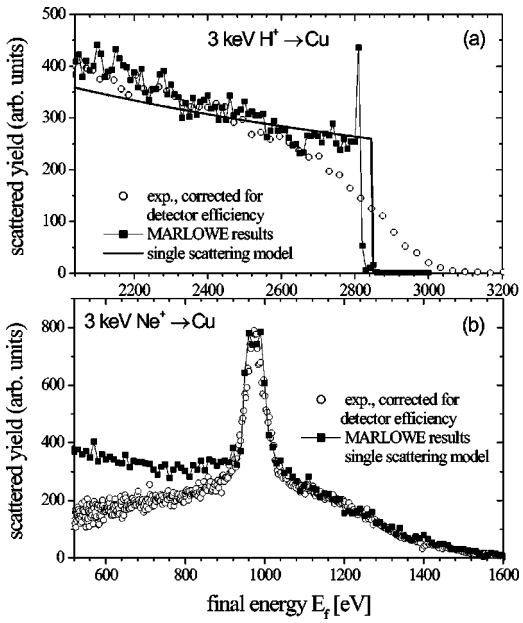

FIG. 8. Same as Fig. 6 for 3-keV H^+ and Ne^+ projectiles.

from the scattering from the surface layer has a very narrow energy width ($\Omega_1 < \Omega_{n>1}$) and (ii) its energy separation from the peak corresponding to the second layer is reduced compared to the other peaks ($dE/dx|_1 < dE/dx|_{n>1}$). Both facts are partly due to the absence of MS in the surface, and partly due to the local electronic energy-loss model used in the simulation.

The experimental spectra are shifted with respect to the original data (see Fig. 5) so that the experimental surface peak coincides with the simulated one, which is always lower than kE_0 due to the use of the inelastic energy-loss model by Oen and Robinson [24] (e.g., 14 eV for 1-keV He and Cu). Both, experiment and simulation extend to the en-

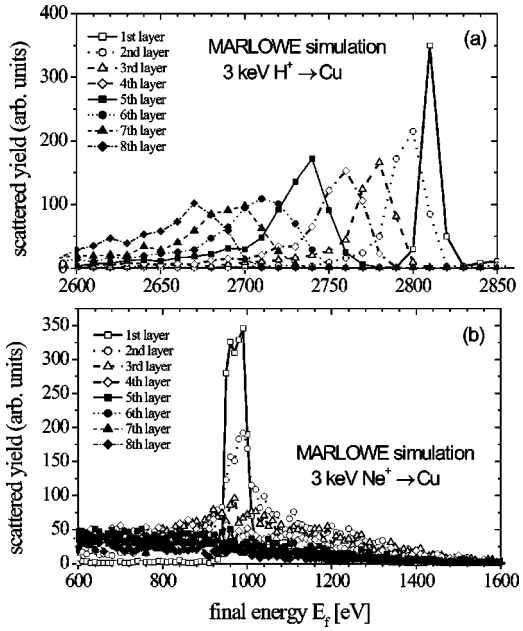

FIG. 9. Same as Fig. 7 for 3-keV H^+ and Ne^+ projectiles.

ergies far above the kinetic single collision limit kE_0, due to PS and MS, and show a pronounced surface peak at kE_0. The surface peak is—as for protons and He ions—due to a reduced energy width of the surface contribution ($\Omega_1 < \Omega_{n>1}$) and due to a reduced energy separation between the first and the second layer ($dE/dx|_1 < dE/dx|_{n>1}$) in the simulation, with the main contribution from the surface layer and the minor contribution from the second layer [see Fig. 9(b)]. That the intensity in the experimental surface peak agrees well with that in the simulation reflects the fact that under the given conditions the onset of PS and MS in the deeper layers is the major reason for the appearance of the surface peak. The reason why there is a discrepancy between the experiment and the simulation at low energies is probably either due to inadequate correction for the detection efficiency or due to deficiencies in the simulation model.

IV. CONCLUSIONS

Charge-integrated scattering spectra in the LEIS exhibit a surface peak in many experimental conditions. We have shown that the appearance of this peak is partly due to a reduced energy width of the contribution from the surface layer ($\Omega_1 < \Omega_{n>1}$) and partly due to a reduced energy loss in the surface layer as compared to the deeper layers ($dE/dx|_1 < dE/dx|_{n>1}$). In the regime of strong multiple scattering, both reasons reflect the fact that scattering from the surface atoms occurs practically exclusively by single binary collisions, while plural scattering and multiple scattering occur in the deeper layers. As a consequence, only the surface layer and to some extent also the second layer will contribute to the surface peak. Experiment as well as simulation show this behavior, so that other possible reasons for the appearance of a surface peak (e.g., channeling) can safely be ruled out.

At high energies, when the multiple-scattering half-width angle $\alpha_{1/2}$ is small, surface effects are mainly caused by electronic stopping and become small, as observed in both the experiment and the simulation. In this regime, the energy spectrum is well described by the single scattering spectrum.

ACKNOWLEDGMENTS

This project was partially supported by the Austrian Science Fund (FWF) (Grant No. P12471-NAW). Inspiring discussions with H.H. Brongersma and W. Heiland are gratefully acknowledged.

[1] E. Taglauer, in *Surface Analysis—The Principal Techniques*, edited by J. C. Vickerman (Wiley-VCH, Weinheim, 1997).
[2] L. Palmetshofer, in *Surface and Thin Film Analysis*, edited by H. Bubert and H. Jenett (Wiley-VCH, Weinheim, 2002), p. 141.
[3] O. Benka, in *Surface and Thin Film Analysis* (Ref. [2]), p. 160.
[4] P. Bauer, in *Surface and Thin Film Analysis* (Ref. [2]), p. 150.
[5] J.A. Leavitt, L.C. McIntire, and M.R. Weller, in *Handbook of Modern Ion Beam Materials Analysis*, edited by J. R. Tesmer and M. Nastasi, Mater. Res. Soc. Symp. Proc. (Materials Research Society, Pittsburgh, 1995), p. 37.
[6] J. F. Ziegler, J. P. Biersack, and U. Littmark, *The Stopping and Range of Ions in Solids* (Pergamon, New York, 1985), Vol. 1.
[7] P. Sigmund and B. Winterbon, Nucl. Instrum. Methods **119**, 541 (1974); **125**, 491 (1975).
[8] J. A. Davies, W. N. Lennard, and I. V. Mitchell, in *Handbook of Modern Ion Beam Materials Analysis* (Ref. [5]), p. 343.
[9] Z. Smit, Phys. Rev. A **48**, 2070 (1993).
[10] T. Buck, G.H. Wheatley, D.P. Jackson, A.L. Boers, S. Luitjens, E. Van Loenen, A.J. Algra, W. Eckstein, and H. Verbeek, Nucl. Instrum. Methods Phys. Res. **194**, 649 (1982).
[11] R.S. Bhattacharya, W. Eckstein, and H. Verbeek, Surf. Sci. **93**, 562 (1980).
[12] E. Rauhala, in *Handbook of Modern Ion Beam Materials Analysis* (Ref. [5], p. 3.
[13] I.C. Vickridge and G. Amsel, Nucl. Instrum. Methods Phys. Res. B **108**, 403 (1996).
[14] M. Draxler, S. N. Ermolov, K. Schmid, C. Hesch, A. Poschacher, R. Gruber, M. Bergsmann, and P. Bauer, in Proceedings of the 15th International Conference on Ion-Surface Interactions (ISI-2001), 2001, Zvenigorod, Moscow District, Russia (unpublished).
[15] K. Schmid, Diploma thesis, University of Linz, 1998 (unpublished).
[16] A. Poschacher, Diploma thesis, University of Linz, 2001 (unpublished).
[17] R. Cortenraad, A.W. Denier van der Gon, and H.H. Brongersma, Surf. Interface Anal. **29**, 524 (2000).
[18] Manual: Channel plate charged particle detectors, model CP-618C, p. 7, Comstock Inc.
[19] M. Draxler, R. Gruber, H.H. Brongersma, and P. Bauer, Phys. Rev. Lett. **89**, 263201 (2002).
[20] T. Buck, G.H. Wheatley, G.L. Miller, D.A.H. Robinson, and Y.S. Chen, Nucl. Instrum. Methods **149**, 591 (1978).
[21] M. Barat, J.A. Fayeton, and Y.J. Picard, Rev. Sci. Instrum. **71**, 2050 (2000).
[22] E. Steinbauer (private communication).
[23] M.T. Robinson and I.M. Torrens, Phys. Rev. B **9**, 5008 (1974).
[24] O.S. Oen and M.T. Robinson, Nucl. Instrum. Methods **132**, 647 (1976).